Radial and Elliptic Flow at RHIC: Further Predictions

P. Huovinen[a], P.F. Kolb[b,c], U. Heinz[b], P.V. Ruuskanen[d], and S.A. Voloshin[e]

[a]Lawrence Berkeley National Laboratory, Berkeley CA 94720, USA

[b]Department of Physics, The Ohio State University, 174 West 18th Avenue, Columbus, OH 43210, USA

[c]Institut für Theoretische Physik, Universität Regensburg, D-93040 Regensburg, Germany

[d]Department of Physics, University of Jyväskylä, FIN-40341 Jyväskylä, Finland

[e]Department of Physics and Astronomy, Wayne State University, 666 W. Hancock Street, Detroit, MI 48202, USA

(February 1, 2008)

Using a hydrodynamic model, we predict the transverse momentum dependence of the spectra and the elliptic flow for different hadrons in Au+Au collisions at $\sqrt{s} = 130\,A$ GeV. The dependence of the differential and p_t-integrated elliptic flow on the hadron mass, equation of state and freeze-out temperature is studied both numerically and analytically.

1. Introduction.– One of the first observables measured at the Relativistic Heavy Ion Collider (RHIC) was the so-called elliptic flow [1]. It describes the azimuthal momentum space anisotropy of particle emission from non-central heavy-ion collisions in the plane transverse to the beam direction. Elliptic flow is characterized by the second harmonic coefficient $v_2(\mathrm{y}, p_t)$ of an azimuthal Fourier decomposition of the momentum distribution [2,3]. We here discuss elliptic flow at midrapidity, $\mathrm{y} = 0$; its p_t-averaged value is denoted simply by v_2.

Elliptic flow is a fundamental observable since it directly reflects the rescattering among the produced particles. Rescattering transfers the initial spatial anisotropy of the nuclear overlap region in the transverse plane to the observed momentum distribution. For a given initial spatial deformation, the largest elliptic flow coefficient is obtained in the hydrodynamic limit where rescattering is so intense that the matter in the reaction zone reaches a state of local thermal equilibrium. Since the spatial anisotropy is largest at the beginning of the evolution, elliptic flow is especially sensitive to the early stages of system evolution [5,6]. A measurement of v_2 thus provides access to the fundamental thermalization time scale in the early stages of a relativistic heavy-ion collision [7,8].

In a preceding Letter we showed [9] that the first measurements at RHIC of the elliptic flow of charged particles can be satisfactorily described by a hydrodynamical model, with initial and freeze-out conditions obtained by a straightforward extrapolation from a similar analysis of Pb+Pb collisions at the SPS [6,8]. The data deviate, however, from the hydrodynamical prediction at large impact parameters $b \gtrsim 7$ fm, where the reaction volumes become small, and at large transverse momenta $p_t \gtrsim 1.5\,\mathrm{GeV}/c$. At the lower SPS energies ($\sqrt{s} = 17\,A$ GeV) the available data [10,11] are less conclusive, but indicate discrepancies with the hydrodynamic approach for all but nearly central collisions [9,12]. Whereas in [1,9] the deviations from hydrodynamic predictions were interpreted to signal incomplete thermalization, the authors of [12] suggest (at least in connection with the SPS data) that they may be due to the transition from an early hydrodynamic to a late hadronic kinetic stage, modeled by a hadronic cascade (RQMD) which leads to an earlier saturation of both radial and elliptic flow.

In the present paper we present hydrodynamic predictions at $\sqrt{s} = 130\,A$ GeV for the shape and impact parameter dependence of the single particle spectra and for the magnitude and p_t-dependence of the elliptic flow for a variety of hadron species. Such data should soon become available. They will not only provide evidence for the degree of thermalization of other hadronic species and thus provide valuable input for the discussion of the two different interpretations just mentioned [9,12], but also help to select between the different combinations of initial and freeze-out conditions and equations of state studied in [9].

2. Hydrodynamic Results.– The hydrodynamic code, its initialization and the calculation of final state spectra and elliptic flow coefficients are described in [8,9]. We here use the parameter sets given in the last three columns of Table I in [9] and label the results accordingly by EOS Q(120), EOS Q(140), and EOS H(140), respectively. EOS H is a hadron resonance gas equation of state with sound velocity $c_\mathrm{s} \approx \sqrt{0.15}$; EOS Q includes a first order phase transition to an ideal quark-gluon gas ($c_\mathrm{s} = \sqrt{1/3}$) at $T_\mathrm{c} = 164$ MeV with a latent heat of 1.15 GeV/fm^3 [13]. In the energy region studied here, EOS Q is effectively softer than EOS H, since the expansion is largely controlled by the soft phase-transition region [8]. Freeze-out is implemented along a surface of constant energy density; the numbers in brackets denote the approximate freeze-out temperature in MeV on this surface.

Radial flow and single-particle spectra: The transverse momentum spectra for negative hadrons, neutral pions and protons are shown in Figure 1. All decay products from strong or electromagnetic decays of unstable resonances up to 1.4 GeV mass are included. These p_t-spectra are considerably flatter than the corresponding SPS spectra; the thin solid lines show our earlier fits [6,8]

to the data from Pb+Pb collisions at $\sqrt{s} = 17\,A\,\mathrm{GeV}$ [14]. This reflects the stronger radial flow at RHIC which hydrodynamics predicts as a result of the higher initial energy density [8]. The crosses in Figure 1 show that the hadronic cascade code UrQMD [15] gives much steeper spectra [16]; in fact, the UrQMD spectra at RHIC energies are slightly steeper than the measured spectra at SPS energies. Apparently the scattering mechanisms built into UrQMD are not efficient enough to build a sufficient amount of radial flow. On the other hand, the flatter slopes of hydrodynamic pion spectra are consistent with first preliminary data on negative hadron spectra at midrapidity [17]. The final data are expected to be accurate enough to distinguish between the three parameter sets shown in Figure 1 (or exclude all of them).
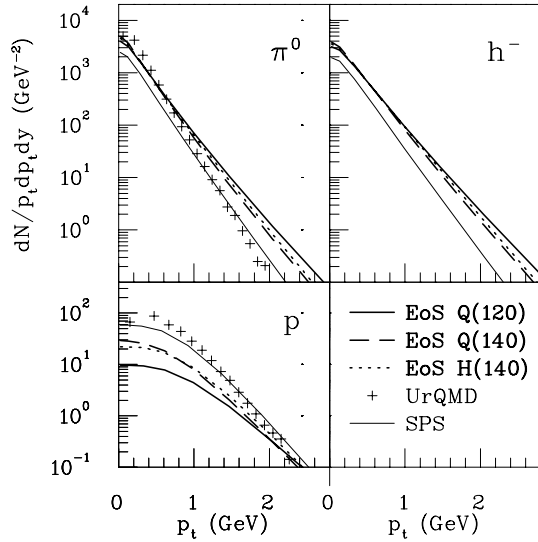

FIG. 1. The p_t spectra of neutral pions (upper left), negative hadrons (upper right), and protons (lower left) for the 6% most central Au+Au collisions at $\sqrt{s} = 130\,A\,\mathrm{GeV}$, for different equations of state and freeze-out temperatures (see text). The crosses show UrQMD results for neutral pions and protons at $\sqrt{s} = 200\,A\,\mathrm{GeV}$ [16] for comparison. Also shown are the corresponding hydrodynamic spectra at $\sqrt{s} = 17\,A\,\mathrm{GeV}$ for EOS Q(120) (thin solid lines).

Figure 2 shows m_t-spectra for pions, kaons, protons and Ω hyperons at different collision centralities. For peripheral collisions the spectra get steeper, due to a decrease of the average radial flow velocity $\langle v_\perp \rangle$ as a result of a lower initial energy density and a shorter lifetime of the reaction zone. The comparison between theory and experiment will be particularly interesting in the region of large impact parameters where the measured elliptic flow [1] lags behind the hydrodynamical results [9]. As discussed in the Introduction, the single-particle spectra may help to understand whether the origin of this discrepancy is incomplete thermalization at an early or late stage of the evolution.
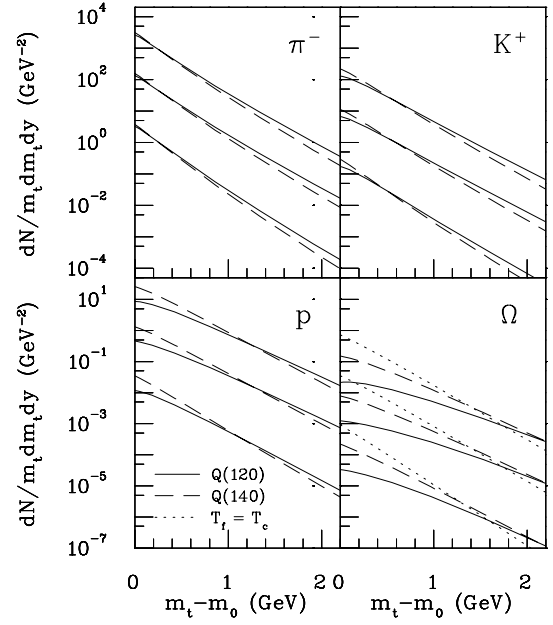

FIG. 2. The m_t-spectra of negative pions (upper left), kaons (upper right), protons (lower left) and Ω baryons (lower right) for Au+Au collisions at $\sqrt{s} = 130\,A\,\mathrm{GeV}$, for collision centralities (top to bottom) $b < 5.4$, $5.4 < b < 9.9$ and $9.9 < b < 13.5$ fm. For clarity the spectra for different centrality bins are separated by factors of 10. The calculations were done with EOS Q. The Ω distribution is also shown for $T_f = 164$ MeV to simulate decoupling at the phase transition.

EOS	Q	Q	H
T_f (MeV) $\approx$	120	140	140
π^-	4.4%	3.6%	4.2%
K^+	5.3%	4.7%	5.7%
p	5.9%	5.3%	6.6%
ϕ	6.2%	5.6%	6.9%
$\phi(T_f=164\,\mathrm{MeV})$	3.8%	3.8%	-
Λ	6.1%	5.6%	7.0%
Ω	6.5%	6.2%	7.7%
$\Omega(T_f=164\,\mathrm{MeV})$	4.4%	4.4%	-

Table 1. Elliptic flow coefficient v_2 at midrapidity for various hadron species from minimum bias Au+Au collisions at $\sqrt{s} = 130\,A\,\mathrm{GeV}$. The p_t-average was taken over the full spectrum.

Elliptic flow. The impact parameter and p_t dependence of the elliptic flow coefficient v_2 for charged particles from Au+Au collisions at $\sqrt{s} = 130\,A\,\mathrm{GeV}$ was discussed in [9]. Table 1 shows predictions for the p_t-integrated elliptic flow of a variety of identified hadrons in minimum bias collisions, for the same three parameter sets as studied in that paper. For the ϕ meson and the Ω hyperon we include two values, one for simultaneous freeze-out with all other hadrons, the other for freeze-out directly after hadronization at $T_c = 164$ MeV. The latter option accounts for the expectation that the

heavy and weakly coupled Ω is not likely to participate after hadronization in any modifications of the previously established flow pattern [18]. Similar arguments hold for the ϕ meson. Even though at RHIC energies a large fraction of the flow is already established before hadronization [8], the additional flow generated afterwards by hadronic rescattering is seen to affect the Ω quite strongly, for both v_2 (Table 1) and the single-particle slope (Figure 2).

For identified pions the dependence of v_2 on EOS and T_f is similar as for the sum of all charged hadrons (see [9]): Lower freeze-out temperatures and harder EOS lead to flatter single particle spectra and thereby to larger p_t-integrated elliptic flow. For identified hadrons we see that, as their mass increases, there is stronger sensitivity to the EoS than that to T_f (see also Figure 4 below).
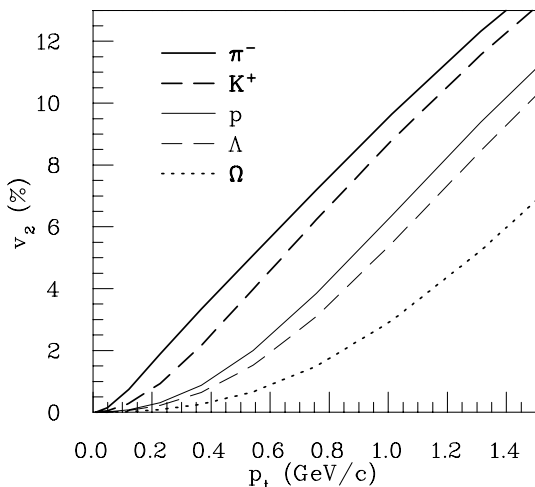

FIG. 3. p_t-differential elliptic flow at midrapidity for various hadrons from minimum bias Au+Au collisions at $\sqrt{s} = 130\,A\,\mathrm{GeV}$ for EOS Q(120).

Figure 3 shows the differential momentum anisotropy $v_2(p_t)$ for different hadron species for EOS Q and $T_f \approx 120\,\mathrm{MeV}$. At a given value of p_t, the elliptic flow is seen to decrease with increasing particle mass. This is a consequence of rest-mass-dependent radial flow effects on the shape of the single-particle p_t-spectrum, as will be analytically discussed in the following section.

The smaller differential anisotropy at fixed p_t does not contradict the results in Table 1 which generically give larger p_t-averaged elliptic flow for heavier particles. This is a consequence of the fact that *radial* flow leads to a flattening of the p_t-spectra of heavier particles [19,20], whose p_t-averaged v_2 thus receives more weight from the high-p_t region where $v_2(p_t)$ is larger. Whether this larger spectral weight for high p_t wins over the reduction of v_2 at fixed p_t depends on the details of the expansion dynamics.

The effect of the EOS and the freeze-out temperature on the differential elliptic flow of pions and protons is

demonstrated in Figure 4. The EOS affects $v_2(p_t)$ for all hadrons in the same way: the stiffer EOS H leads to larger v_2 at low p_t and to smaller v_2 at high p_t than the softer EOS Q. The effect of the freeze-out temperature on $v_2(p_t)$ is more delicate: for pions the effect is small, and for EOS Q an increase in the freeze-out temperature decreases both the p_t-averaged and the differential elliptic flow. The heavier protons behave oppositely: the differential anisotropy increases with increasing freeze-out temperature. The origin of this behaviour will be studied in the following section. Clearly, the different T_f-dependence of $v_2(p_t)$ of different particles can be used to constrain the freeze-out temperature independently of the EOS.
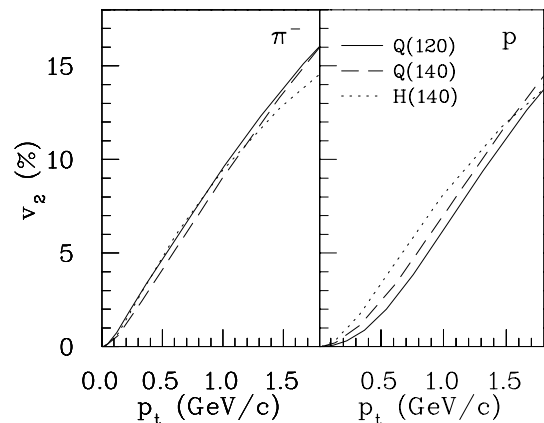

FIG. 4. The effect of the EOS and the freeze-out temperature on the elliptic flow of midrapidity pions (left) and protons (right) from minimum bias Au+Au collisions at $\sqrt{s} = 130\,A\,\mathrm{GeV}$.

In view of the observed deviations from hydrodynamic behaviour of charged particle elliptic flow at large impact parameters [1] it will be interesting to study the centrality dependence of v_2 separately for a variety of hadron species. Corresponding hydrodynamic predictions are shown in Figure 5 (again including the option that the Ω freezes out early at $T_f = T_c$). Particle-specific deviations from these predictions should provide valuable insights into the thermalization and freeze-out mechanisms.

3. Analytical results.– In the remainder we try to understand the hydrodynamic behaviour of $v_2(p_t)$ and its dependence on the hadron mass and freeze-out temperature, using a simple analytical model. Before going into the technical details we give a simple intuitive argument why, at small p_t, the elliptic flow of heavier particles is smaller than for lighter ones. It is well-known that radial flow shifts the p_t-distributions to larger values of p_t, and that for nonrelativistic $p_t < m$ this effect increases with the particle mass m and the radial flow velocity $\langle v_\perp \rangle$. In the extreme case of a thin shell expanding at high velocity, the spectrum actually develops a relative minimum at $p_t = 0$ and a peak at nonzero p_t ("blast wave peak"

[19]), and with increasing mass and $\langle v_\perp \rangle$ the peak shifts to larger p_t. Relative to the case without radial flow, the spectrum is thus depleted at small p_t, and the depletion as well as the p_t range over which it occurs increase with m and $\langle v_\perp \rangle$.
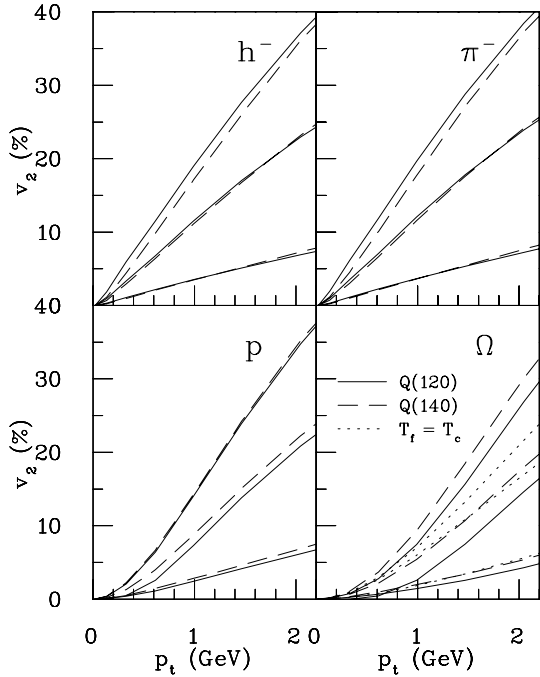

FIG. 5. The p_t-differential elliptic flow of negative hadrons (upper left), pions (upper right), protons (lower left) and omega baryons (lower right) for Au+Au collisions at $\sqrt{s} = 130\,A\,\text{GeV}$ for collision centralities (top to bottom) $9.9 < b < 13.5$, $5.4 < b < 9.9$ and $b < 5.4$ fm. The calculations were done for EOS Q.

If, as in the case of fully developed elliptic flow, the radial velocity is larger in x than in y direction, $|v_x| > |v_y|$, the same is true for this relative depletion effect. It counteracts the excess of particles with p_t in x-direction over those with p_t in y-direction which is the origin of $v_2 > 0$. Thus it reduces v_2 at small p_t. This reduction and the p_t-range over which it occurs both increase with the particle mass m and the average radial flow $\langle v_\perp \rangle$. A quick graphic sketch shows that in the extreme case, where the single-particle spectrum develops a "blast wave peak" [19], v_2 even turns negative at low p_t, due to the shift of the peak to larger p_t in x than in y direction if $|v_x| > |v_y|$.

When looking for a simple model which allows to show this analytically, a generalization of the "blast wave" model [19] comes to mind, in which thermalized matter of temperature T_f, approximated by a boosted Boltzmann distribution, freezes out on a thin cylindrical shell along which the radial flow shows an azimuthal modulation with $|v_x| > |v_y|$. Assuming boost-invariant longitudinal expansion and freeze-out at constant proper time,

the Cooper-Frye freeze-out spectrum can be calculated by trivially generalizing the derivation given in [21,22]. In the Boltzmann approximation[1] one finds, up to irrelevant constants,

$$\frac{dN}{dy\, dm_t^2\, d\phi_p} \sim \int_0^{2\pi} d\phi_s\, K_1(\beta_t(\phi_s))\, e^{\alpha_t(\phi_s)\cos(\phi_s - \phi_p)}, \quad (1)$$

where ϕ_s, ϕ_p are the azimuthal angles in coordinate and momentum space, and the arguments $\alpha_t(\phi_s) = (p_t/T)\sinh(\rho(\phi_s))$, $\beta_t(\phi_s) = (m_t/T)\cosh(\rho(\phi_s))$ [22] now depend on a ϕ_s-dependent radial flow rapidity $\rho(\phi_s)$. The elliptic flow coefficient is obtained by taking the azimuthal average over $\cos(2\phi_p)$ with this spectrum, $v_2 = \langle \cos(2\phi_p) \rangle$. The ϕ_p-integral can be done analytically:

$$v_2(p_t) = \frac{\int_0^{2\pi} d\phi_s\, \cos(2\phi_s)\, I_2(\alpha_t(\phi_s))\, K_1(\beta_t(\phi_s))}{\int_0^{2\pi} d\phi_s\, I_0(\alpha_t(\phi_s))\, K_1(\beta_t(\phi_s))}. \quad (2)$$

Making the *Ansatz* $\rho = \rho_0 + \rho_a \cos(2\phi_s)$ we checked that, for a suitable choice of the average radial flow rapidity ρ_0 and its azimuthal modulation amplitude ρ_a, Eq. (2) reproduces all relevant features of the full hydrodynamic results almost quantitatively. The ϕ_s-independent version of Eq. (1) [20] has been used very successfully by many groups to fit single-particle spectra from central heavy-ion collisions in order to extract the average temperature and radial flow velocity at freeze-out. Similarly, Eqs. (1) and (2) can be used to fit the spectra and elliptic flow from non-central collisions in order to extract also the average azimuthal flow modulation.
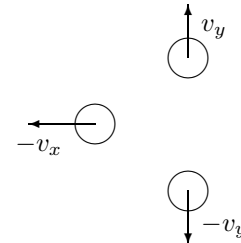

FIG. 6. Simple source of four fireballs.

Unfortunately, the remaining angular integral in (2) cannot be done analytically. To reach a fully analytical understanding of many of the features observed in the previous section one can exploit an even simpler model which still captures the main effects qualitatively, but no longer quantitatively. It consists of four non-expanding fireballs of equal volume, freezing out instantaneously

---

[1]For Bose-Einstein or Fermi-Dirac distributions, one simply substitutes Eq. (1) by a sum of terms with T replaced by T/n, $n = 1, 2, \ldots$, and weighted with $(\pm 1)^n$ [21].

and simultaneously in the laboratory frame, whose centers move in the transverse plane without longitudinal velocity component (see Fig. 6). What matters for the observed particle flow pattern are the velocities of the four fireballs, as indicated in the figure, but not their positions nor the size of their common laboratory frame volume.

For this model one finds, again in the Boltzmann approximation, the simple expression

$$v_2(\mathrm{y}, p_t) = \frac{I_2\left(\frac{\gamma_x v_x p_t}{T}\right) - e^{\frac{E}{T}(\gamma_x - \gamma_y)} I_2\left(\frac{\gamma_y v_y p_t}{T}\right)}{I_0\left(\frac{\gamma_x v_x p_t}{T}\right) + e^{\frac{E}{T}(\gamma_x - \gamma_y)} I_0\left(\frac{\gamma_y v_y p_t}{T}\right)}. \qquad (3)$$

In this equation the particle mass enters only in the term $e^{\frac{E}{T}(\gamma_x - \gamma_y)}$, and it is easy to see that if all other variables are held fixed, v_2 decreases with increasing mass. Figure 7 shows that our schematic source also reproduces the feature of negative v_2 for protons at small p_t which was anticipated above from the "blast wave" model. (This feature is also preserved by the cylindrical shell model, Eq. (2).) The "blast wave peak" in the single-particle spectrum is known to disappear when the constant expansion velocity is replaced by a realistic radial velocity distribution [20]; we therefore then also expect the dip of v_2 to negative values to be washed out, in agreement with Figs. 3 and 4. On the other hand, the UrQMD calculations reported in [23] do show negative v_2 for midrapidity protons at small p_t; it would be interesting to further investigate the origin of this effect in that model. It may be worth pointing out that a similar interplay between radial flow, random thermal motion and a *directed* flow anisotropy (first instead of second harmonic modulation) has been shown [24] to be responsible for negative directed flow coefficients v_1 at low p_t [10].
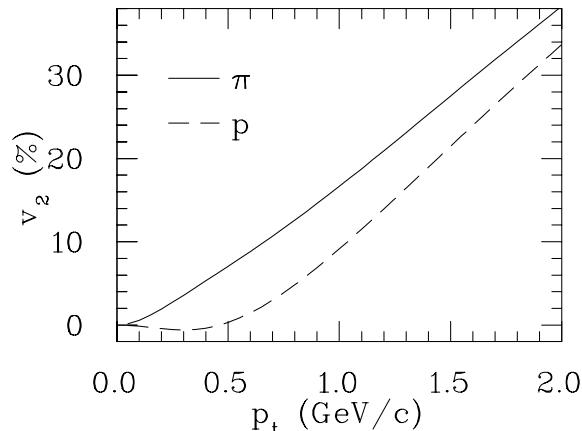

FIG. 7. Transverse momentum dependence of elliptic flow for midrapidity pions and protons from the schematic source in Figure 6, for $T = 140\,\mathrm{MeV}$, $v_x = 0.6$, and $v_y = 0.5$.

Our schematic source also permits us to understand the approximately linear p_t-dependence of v_2 in the intermediate p_t region. Expanding the Bessel functions in

(3) for large arguments and keeping only the leading term gives for midrapidity (y=0) particles

$$v_2(p_t) \approx \tanh\left(\frac{1}{2}\left(\frac{\kappa p_t - \lambda m_t}{T} + \mu\right)\right), \qquad (4)$$

where $\kappa = \gamma_x v_x - \gamma_y v_y$, $\lambda = \gamma_x - \gamma_y$ and $\mu = \ln(\sqrt{\frac{\gamma_x v_x}{\gamma_y v_y}})$. Since $\kappa > \lambda$ for $|v_x| > |v_y|$, we get for $p_t \gg m$ the simple form $v_2(p_t) \approx \tanh(\xi p_t)$ with $\xi = (\kappa - \lambda)/2T$. For the example in Fig. 7, $\xi \approx 5\,\mathrm{GeV}$, and v_2 begins to turn over at $p_t > 2.5\,\mathrm{GeV}$, saturating at $v_2 = 1$ as $p_t \to \infty$. This consideration also shows that the scale at which v_2 changes from its required quadratic p_t-dependence at low p_t [25] (with a positive or negative coefficient) to a linear behaviour at intermediate p_t is given by the particle rest mass m, multiplied by a prefactor of order 1 which is governed by the average radial flow velocity $\langle v_\perp \rangle$.

We finally discuss the dependence of v_2 on the freeze-out temperature. Taking the temperature derivative of Eq. (4) we get (again at y=0)

$$\frac{\partial v_2}{\partial T}(p_t) \approx \frac{\lambda m_t - \kappa p_t}{2T^2} \frac{1}{\cosh^2\left(\frac{1}{2}\left(\frac{\kappa p_t - \lambda m_t}{T} + \mu\right)\right)}. \qquad (5)$$

With $\kappa > \lambda$ one sees that at fixed p_t the sign of the derivative depends on the particle mass and that, for increasing T_f, $v_2(p_t)$ may thus decrease for pions while increasing for protons, as seen in Fig. 4.[2]

4. Summary.– We have presented a variety of predictions for the elliptic flow and single-particle spectra for different hadron species produced in Au+Au collisions at $\sqrt{s} = 130\,A\,\mathrm{GeV}$, using a relativistic hydrodynamic model. We have studied the sensitivities to the equation of state and freeze-out temperature and showed that these can be used to further constrain the model parameters and test the approach on a quantitative level. A simple expression for fitting spectra and elliptic flow data in order to extract the average radial flow and flow anisotropy has been given. Crucial features of the p_t-dependence of the elliptic flow have been elucidated with a simple schematic model. Testing the predicted p_t-dependence of v_2 for many different hadron species will clarify the validity of the picture of a thermalized expanding source with a common flow velocity for all hadrons at RHIC energies.

---

[2]Of course, in a full hydrodynamic calculation T_f cannot be varied independently of the flow velocities, and the latter are not fixed, but vary over the freeze-out surface. Eq. (5) can only give a qualitative impression.

[1] K.H. Ackermann *et al.* (STAR Collaboration), Phys. Rev. Lett. **86** (2001) 402.

[2] J.-Y. Ollitrault, Phys. Rev. D **46** (1992) 229.

[3] S.A. Voloshin and Y. Zhang, Z. Phys. C **70** (1996) 665.

[4] S.A. Voloshin and A.M. Poskanzer, Phys. Lett. B **474** (2000) 27.

[5] H. Sorge, Phys. Rev. Lett. **78** (1997) 2309; **82** (1999) 2048.

[6] P.F. Kolb, J. Sollfrank and U. Heinz, Phys. Lett. B **459** (1999) 667; P.F. Kolb, J. Sollfrank, P.V. Ruuskanen, and U. Heinz, Nucl. Phys. **A661** (1999) 349.

[7] S.A. Voloshin and A.M. Poskanzer, Phys. Lett. B **474** (2000) 27.

[8] P.F. Kolb, J. Sollfrank, and U. Heinz, Phys. Rev. C **62** (2000) 054909.

[9] P.F. Kolb, P. Huovinen, U. Heinz, and H. Heiselberg, hep-ph/0012137, Phys. Lett. B, in press.

[10] H. Appelshäuser *et al.* (NA49 Collaboration), Phys. Rev. Lett. **80** (1998) 4136 and the NA49 home page http://na49info.cern.ch/na49/Archives/Images/Publications/

[11] A. Poskanzer and S. Voloshin for the NA49 Collaboration, Nucl. Phys. **A661** (1999) 341c.

[12] D. Teaney, J. Laurent, and E.V. Shuryak, nucl-th/0011058.

[13] J. Sollfrank *et al.*, Phys. Rev. C **55** (1997) 392.

[14] H. Appelshäuser *et al.* (NA49 Collaboration), Phys. Rev. Lett. **82** (1999) 2471.

[15] S.A. Bass *et al.*, Prog. Part. Nucl. Phys. **41** (1998) 225; M. Bleicher *et al.*, J. Phys. G 25 (1999) 1859.

[16] M.J. Bleicher *et al.*, Phys. Rev. C **62** (2000) 024904.

[17] Preliminary results reported by the STAR Collaboration at DNP2000, see http://www-rnc.lbl.gov/STAR/conf/talks2000/dnp/ullrich.html

[18] H. van Hecke, H. Sorge, and N. Xu, Phys. Rev. Lett. **81** (1998) 5764.

[19] P.J. Siemens and J.O. Rasmussen, Phys. Rev. Lett. **42** (1979) 880.

[20] K.S. Lee, U. Heinz, and E. Schnedermann, Z. Phys. C **48** (1990) 525.

[21] P.V. Ruuskanen, Acta Phys. Pol. **18** (1988) 551.

[22] U. Heinz, K.S. Lee, and E. Schnedermann, in: *Quark-Gluon Plasma* (R.C. Hwa, ed.), Advanced Series on Directions in High Energy Physics, Vol. 6, p. 471 (World Scientific, Singapore, 1990).

[23] M. Bleicher and H. Stöcker, hep-ph/0006147.

[24] S.A. Voloshin, Phys. Rev. C **55** (1997) 1630.

[25] P. Danielewicz, Phys. Rev. C **51** (1995) 716.